

Radiation Physics and Engineering 2023; 4(2):9–17

Studying the effect of backgrounds on the determination of radiative thermal neutron capture cross-section in the Neutron Powder Diffraction facility of the Tehran Research Reactor

Mahya Pazoki^a, Hamid Jafari^{a,*}, Zohreh Gholamzadeh^b

^aDepartment of Radiation Application, Shahid Beheshti University, Tehran, Iran

^bReactor and Nuclear Safety, Nuclear Science and Technology Research Institute, Atomic Energy Organization of Iran, Tehran, Iran

HIGHLIGHTS

- Flux distribution and its effect on the numerical value of the cross-section has been investigated.
- Neutron Powder Diffraction facility of Tehran Research Reactor were considered as a neutron source.
- Background effects on the calculated cross-sections were compared to the results of the EXFOR data library.
- Foils of gold, indium, and rhodium have been used as the samples irradiated by monochromatic neutron beam.

ABSTRACT

Neutron data and cross-sections are highly regarded and are essential for developing nuclear equipment such as advanced fission and fusion reactors, accelerators, neutron shielding, physics studies, etc. The neutron cross-section should preferably be measured using a single-energy neutron beam, although the presence of a background in research reactors can affect its accurate determination. The Neutron Powder Diffraction (NPD) facility of Tehran Research Reactor (TRR) has been taken into consideration for measuring the neutron cross-section based on its properties, including neutron monochromator and multiple collimators. In this work, radiative capture cross-sections of Au, In, and Rh materials have been calculated using TRR monochromatic beam. MCNPX is a Monte Carlo particle transport code that has been applied to simulate the measurement system of the neutron cross-section and calculate the reaction rates. The effect of the presence and absence of different sections of the background on the cross-section values was investigated and the results were compared with EXFOR data library for validation. According to the findings, neutron backgrounds can have varying impacts depending on factors such as sample material, the isotope resonance regions, neutron source spatial distribution, and neutron monochromatic energy. However, the presence of fast neutron background contributes to the most uncertainty in the cross section values while its removal produces an average discrepancy from experimental libraries of 7.16%. Also, removing the cold neutron background also causes a relative difference equal to 7.65%.

KEYWORDS

Cross-section
Neutron activation
TRR
MCNPX
Monochromatic beam

HISTORY

Received: 30 June 2022
Revised: 5 August 2022
Accepted: 18 August 2022
Published: Spring 2023

1 Introduction

The importance of neutron reaction cross-section data in the research and development of nuclear technologies is well known. Neutron cross-sections are the key quantities required to calculate neutron reactions taking place in reactors, shielding, transmutation process, detecting, space application, etc. (Huang et al., 1998; Rubbia et al., 1995). In this regard, the thermal neutron cross-section is the

most important particularly for neutron absorber materials. These materials reduce exposure to neutron radiation. They are suitable for applications using neutron emitting sources: nuclear industry, cyclotron, medical accelerator, etc. (Lamarsh et al., 2001). Therefore in recent decades, preparing evaluated cross-section sets has become a discipline in itself and has been developing since the early 1960s. Moreover, neutron activation is one of the most frequently used techniques for neutron cross-section mea-

*Corresponding author: h.jafari@sbu.ac.ir

<https://doi.org/10.22034/rpe.2022.349750.1094>

<https://dorl.net/dor/20.1001.1.26456397.2023.4.2.2.8>

surements (El Abd et al., 2017). Neutron activation analysis (NAA) is a method based on the conversion of stable nuclei to radioactive ones by neutron capture. The essence of this method is about the measurement of released radiation from product radioactive nuclei. All of the stable elements are suitable for such a method but depending on the employed instrument, the radioactive product's half-lives should be considered.

A mono-energetic neutron source is the most suitable radiation source to measure the accurate value of material cross-sections. However, the total distribution of a neutron beam can be also applied in special circumstances. In neutron diffractometry facilities, single crystals are usually used as monochromators. Nevertheless, the presence of a radiation background in a monochromatic output beam requires the use of neutron filters to minimize higher-order contaminations. Several materials such as quartz (SiO_2) (Harvey et al., 1988), bismuth (Adib and Kilany, 2003), silicon (Brugger, 1976), lead (Adib et al., 2002), MgO (Adib et al., 2011), and sapphire (Al_2O_3) (Adib, 2005) have been suggested as the most successful filter materials. At high neutron energies, greater than about 1eV, the total neutron cross-section of each of the above-mentioned materials is in the range of a few barns. But at lower thermal energies, less than 0.1 eV, where much of the coherent Bragg scattering is forbidden the effective cross-section for single-crystal specimens is much reduced. Furthermore, iron, beryllium, BeO , and graphite are perhaps the most suitable materials when used as a cold neutron filter (Adib et al., 2004). Researchers in the most of the national laboratories and several the commercial reactor designs have worked on cross-section measurement and many studies have been carried out by NAA procedure which some of them are stated in the following:

Celenk et al. (Celenk et al., 1991) measured the total thermal neutron macroscopic and microscopic cross-sections of V, Co, Cu, In, Dy and Au by using neutron self-absorption properties. 99% pure foils of elements with different thicknesses were utilized. In addition, Pu-Be was applied as a Maxwellian velocity distribution neutron source. The thermal neutron flux was about 10^4 $\text{n.cm}^{-2}.\text{s}^{-1}$ at the irradiation position. All foils of each element were irradiated with and without cadmium cover to determine the epithermal portion of the neutron spectrum. Areas of interest of gamma-photopeak, which were determined from the spectra from the foils, were plotted as foil thickness function. Then, a non-linear least-squares fitting method was applied and the total thermal neutron macroscopic and microscopic cross-section of the elements were obtained. The results were in good agreement with the compiled results by the libraries (Celenk et al., 1991).

Drozdowicz et al. (Drozdowicz, 1989) measured the macroscopic effective absorption cross-section of thermal neutrons in homogeneous and heterogeneous materials. Czubek's pulsed neutron method which is independent of the scattering properties of the sample was used to measure the absorption cross-section. The silicon samples in a cylindrical shape were surrounded by a moderator as only thermal neutrons were desired and covered with a cadmium cover. It has resulted that generally, the

thermal-neutron absorption cross-section of any heterogeneous medium is always lower than a homogeneous one consisting of the same components. Very good agreement was observed between theoretical and experimental results of this work (Drozdowicz, 1989).

A method was developed by Elabd et al. (El Abd et al., 2017) for measuring both thermal neutron macroscopic absorption and scattering cross-sections for any sample in the form of powder or liquid. It is based on a wide beam of a Pu-Be neutron source and He-3 neutron detector assembly. Also, a semi-empirical model was proposed to fit the results. The model successfully fitted the results of both the solid and liquid standard samples (El Abd et al., 2017). Furthermore, Jacobson et al. (Jacobson, 1988) reviewed instrumentations and techniques for measuring thermal neutron capture cross-section in cased wellbores as an important formation evaluation tool for the petroleum industry. They discussed historical development, physical principles, applications, and recent developments in this field, and the importance of neutron macroscopic cross-section in log interpretation (Jacobson, 1988).

The behavior of thermal neutrons of 20 materials consisting of 12 elements, 3 alloys, and 5 chemicals was analyzed by Kobayashi et al. (Kobayashi et al., 1992) by applying the neutron radiography technique with the TRIGA-11 100 kW reactor. Scattering components were estimated and subtracted from the observed neutron intensities measured behind the slabs. A thermal neutron fluence of 2×10^9 n.cm^{-2} was provided at the sample position. Measured values agreed within $\pm 20\%$ with predicted values (Kobayashi et al., 1992).

Due to the need for high accuracy in the cross-section measurement, it is recommended that the situation of the experiment be simulated using Monte Carlo radiation transport calculations before any practical work. Therefore, nuclear models and Monte Carlo based codes are also frequently used to estimate neutron-induced reaction cross-section in those calculations in which no experimental data are available besides neutron cross-section measurement (Cierjacks et al., 1994).

Hancerliogullari et al. (Hancerliogullari et al., 2017) calculated total neutron macroscopic cross-sections based on transmission by Fluka Monte Carlo code and determining minerals, Sussexite and Vimsite, based on new shielding materials against fast neutron particles. The results of this investigation provided new information about the total macroscopic cross-sections, secondary radiation, neutron flow absorbed doses, and deposited energies by low energy neutron interaction of fast neutrons through materials including different amounts of boron and hydrogen atoms per unit volume. It is reported that all three minerals have been identified as a better neutron shield material than concrete (Hancerliogullari et al., 2017).

The development of new materials in the nuclear industry and the necessity of their nuclear data sheet preparation motivates any advanced nuclear center to develop itself neutron cross-section laboratory. TRR has been equipped with a monochromatic neutron beam at the D beam tube which is supposed to be used for measuring the thermal neutron cross-section. In this work, radiative cap-

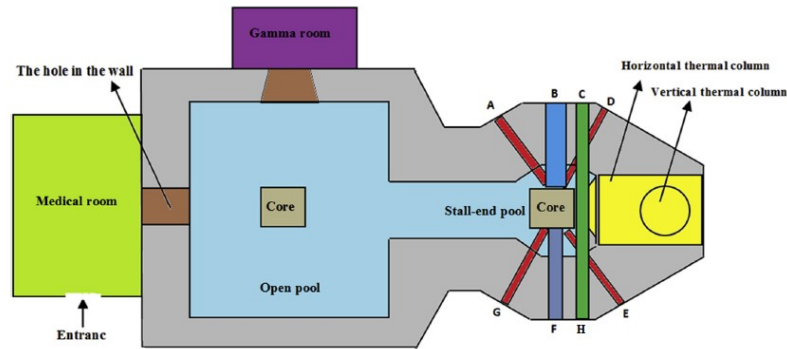


Figure 1: The schematic view of TRR pools and irradiation facilities (Gholamzadeh et al., 2018).

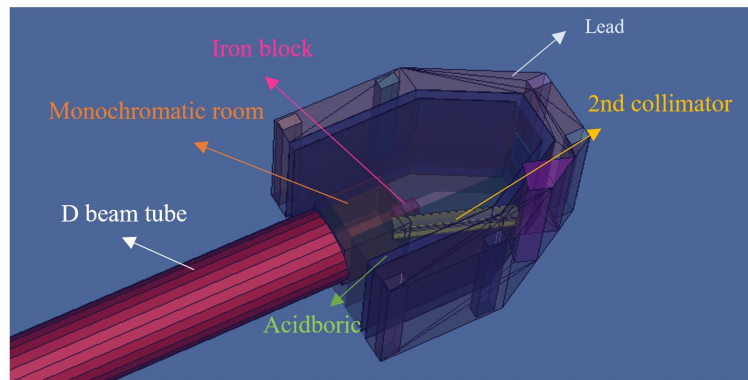


Figure 2: D beam tube arrangement of NPD facility of TRR (Gholamzadeh et al., 2018).

ture cross-sections of Au, In, and Rh materials have been calculated using TRR monochromatic beam. MCNPX is a Monte Carlo particle transport code that has been applied to simulate the measurement system of the neutron cross-section and calculate the reaction rates. Under different conditions, geometries and particle fluxes, MCNPX will estimate the most possible reaction rate based on its experimental data stored in the ENDF library. Therefore, this code is not capable to calculate a microscopic cross-section of an unknown compound material. The neutron cross-section should preferably be measured using a single-energy neutron beam, but in the TRR NPD facility, the presence of neutron backgrounds in the neutron spectrum is observed. Then, the background effects on the calculated cross-sections have been compared to the experimentally measured data obtained from the IAEA-EXFOR library to evaluate the relative discrepancies and consequently determine the most useful neutron filtering of any background section.

2 Materials and Methods

2.1 Description of TRR

TRR is a pool-type light water nuclear reactor in that water acts as both coolant and moderator. Its fuel assemblies contain low-enriched uranium with a 20% concentration of U-235 in the form of U3O8Al alloy. The TRR pool contains two sections. One section called stall-end contains experimental facilities like beam tubes, rabbit system, and

thermal column. The other section is the open end which is designed for bulk irradiation studies. Figure 1 shows a schematic view of the TRR pool and irradiation facilities. As it is shown there are seven beam tubes called A, B, C, D, E, F, and G. These beam tubes are composed of an aluminum chamber and stainless steel housing (Gholamzadeh et al., 2018; Dastjerdi et al., 2016).

2.2 Neutron Powder Diffraction Facility of TRR

D beam tube of TRR provides a monochromatic neutron beam and has been considered a neutron powder diffractometer (NPD) system. This NPD facility includes equipment such as a first collimator, monochromator, neutron and gamma shield, second collimator, sample table, third collimator, and neutron detectors. The first collimator is a rectangular soller-type collimator made of steel with dimensions of $7 \times 11 \times 120 \text{ cm}^3$. A rectangular high ordered pyrolytic graphite (HOPG) monochromator is located along the beamline at the distance of 15 cm from the first collimator exit. The monochromatic beam enters the second collimator, which has dimensions of $6 \times 10 \times 60 \text{ cm}^3$. Different thicknesses of the iron box, paraffin, boric acid powder, and lead surrounded the monochromator room to decrease the neutron and gamma doses. A shutter is placed at the end of the second collimator, which is closed when the beam is not required. The neutron wavelength of the beam can be varied in the range of 0.5 to 3 Å by different angles of placement and rotation of the HOPG crystal (65° , 75° , 80° , and 85°). Maximum neutron flux

on the sample table is obtained at 75° . A schematic of the NPD facility is shown in Fig. 2. In addition, neutron flux as a function of energy after the PG monochromator and at the sample position, which is located 120 cm away from the second collimator is shown in Fig. 3 (Gholamzadeh et al., 2018). The characteristics of this channel make it suitable for use in cross-section measurement.

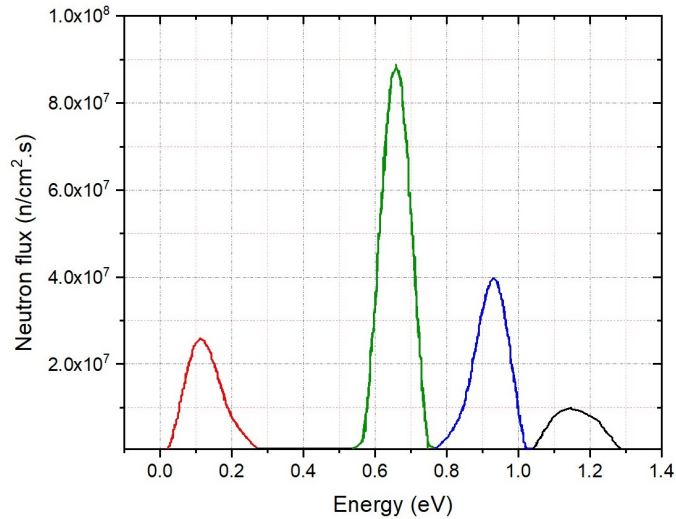


Figure 3: The neutron flux versus energy after the PG monochromator and at the sample position (Gholamzadeh et al., 2018).

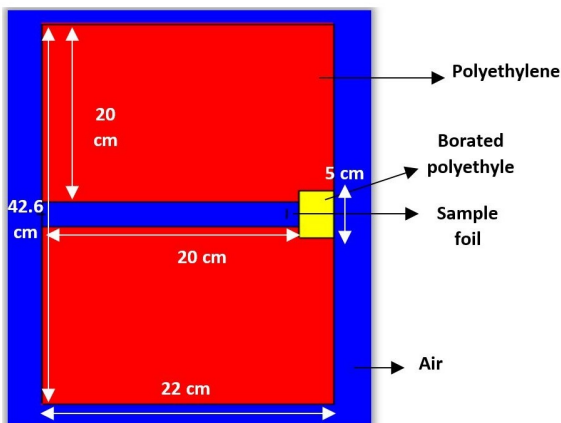
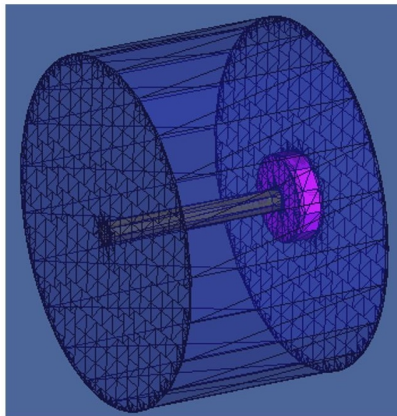


Figure 4: A view of MCNPX simulated geometry and sample position.

2.3 Computational approach

Among all of the capture reactions, (n, γ) reaction is the most important one for activation analysis. It is widely used according to its favorable cross-section, radioactive products with appropriate half-lives, and the ability to be run with any source of thermal neutrons (Steele and Meinke, 1962). To calculate the neutron cross-section by the Monte Carlo method, neutron flux/fluence and the reaction rate/density are required. Radiative capture microscopic cross-section of $\sigma_{(n,\gamma)}$ is obtained by dividing neutron reaction rate ($RR_{n,\gamma}$) by neutron total flux (Φ) and atomic density of the isotope (N) which is given by Eq. (1) (Pelowitz et al., 2011):

$$\sigma_{n,\gamma} = \frac{RR_{n,\gamma}}{\Phi N} \quad (1)$$

Partial cross-sections of isotopes have been measured during recent decades by experimental methods in numerous facilities. By using these experimental data stored in ENDF libraries, as well as information about neutron flux, MCNPX is capable to estimate the desired reaction rate. It should be noted that the MCNPX code cannot calculate the microscopic cross-section directly and this method is unusable for unknown isotopes without any data in the MCNPX library. In this study, different states of the neutron flux after the second collimator of TRR is considered as neutron source.

The MCNPX is a general-purpose Monte Carlo particle transport code that began in 1994 as an extension of MCNP4B and LAHET 2.8 in support of the accelerator production of tritium project (APT) (Pelowitz et al., 2011). The work envisioned a formal extension of MCNP to all particles and all energies; improvement of physics simulation models; extension of the neutron, proton, and photonuclear libraries to 150 MeV; and the formulation of new variance-reduction and data-analysis techniques. The program also included crosssection measurements, benchmark experiments, deterministic code development, and improvements in transmutation code and library tools through the CINDER90 project (Pelowitz et al., 2011, 2005).

The simulated geometry including the sample position at 3 cm away from the end of the D beam tube is shown in Fig. 4. This is a hollow cylinder with depicted dimensions and the sample foil ($1 \times 1 \times 0.001$ cm) is just located in front of a 5% borated-polyethylene as a sample holder. Here, indium (In), gold (Au), and rhodium (Rh) have been selected as the sample foils.

The track length estimator tally (F4) has been used to obtain neutron fluence. Due to the limitation in the optical physics of MCNPX, this is not able to consider monochromator crystal properties in the neutron spectra. Therefore, the monochromatic peaks have been added manually. The properties of these monochromatic peaks including their FWHM were calculated before using the Vitess code (Gholamzadeh et al., 2018).

The final obtained spectra were introduced as an input source for the microscopic cross-section calculation. Moreover, the tally multiplier (FM card) has been used to

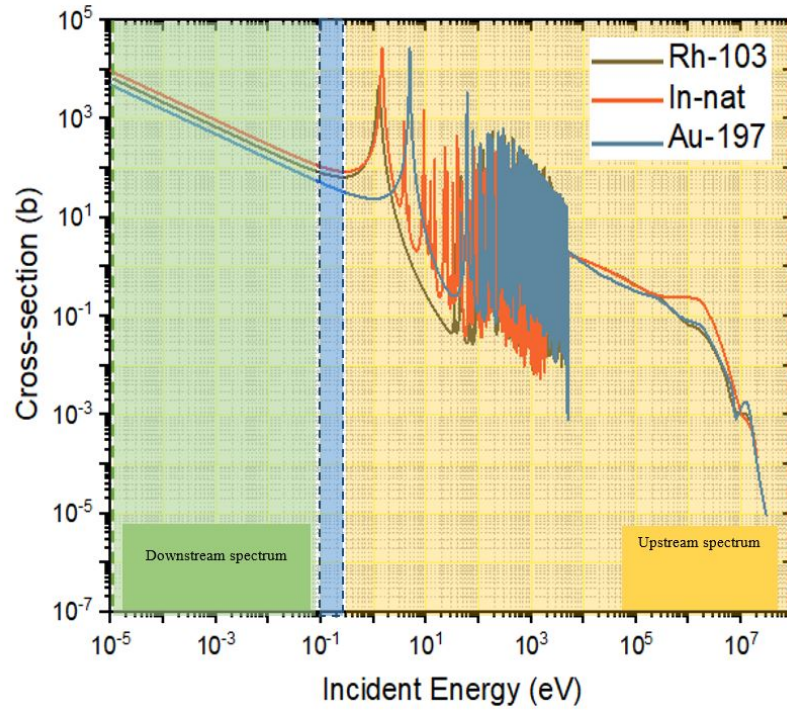


Figure 5: (n, γ) cross-section of three elements of Rh, In, and Au by specifying monochromatic energy interval of TRR NPD facility and upstream and downstream energy ranges (ENDF, 2021).

compute the different neutron reaction rates as Eq. (2) (Pelowitz et al., 2005):

$$RR_i = C \int \Phi(E) \sigma_i(E) dE \quad (2)$$

where $\sigma_i(E)$ is the microscopic cross-section of reaction, $\Phi(E)$ is the neutron flux as a function of energy, and C is the normalized coefficient which may be as atomic density [atoms.b⁻¹.cm⁻¹]. On this occasion, the reaction cross-sections are microscopic with units of barns. Assuming C as constant “1” results in a microscopic cross-section in which the number “-1” specifies a macroscopic scale. The number of histories has been considered so that statistical uncertainty is less than 1%.

As illustrated, the neutron cross-section should preferably be measured using a single-energy neutron beam, but in the TRR NPD facility, the presence of neutron backgrounds in the neutron spectrum is observed. The full spectrum contains a monochromatic peak depending on PG crystal orientation and the energies of 0.331 eV, 0.083 eV, 0.036 eV, 0.020 eV, and 0.013 eV have been considered in this regard. In addition, the effects of removing fast and cold neutron backgrounds on the enhancement of neutron cross-section calculation using the monochromatic beam have been investigated. These two other supposed conditions are the upstream spectrum which removes before the mono-energetic peak and the downstream spectrum which removes after the mono-energetic peak from the full spectrum. Of course, these conditions and the elimination of such species from parts of the spectrum are exaggerated and far from the experimental reality, but in this work, a general estimate has been made to determine the appropriate type of filtration. In this case, a suitable filter can

be designed to measure the cross-section more accurately and in detail in the future.

The neutron capture cross-sections of (n, γ) , corresponding to the three sample materials (In, Au, Rh), are shown in Fig. 5. The cross-section values have been extracted from the nuclear data library of ENDF/BVIII (ENDF, 2021). As seen, the monochromatic intervals (which are possible using the NPD system of TRR) have been depicted in blue color related to the neutron energy range of 0.020 to 0.331 eV. In addition, the upstream and downstream ranges have been shown by yellow and green color regions.

The results of (n, γ) microscopic cross-section calculation for the Au-197 sample which was irradiated by monochromatic neutron beams with a peak at 0.331, 0.083, 0.036, 0.020, and 0.013 eV are given in Tables 1 to 5, respectively. All the results are compared with the EXFOR -Experimental Nuclear Reaction Data- library, which contains an extensive compilation of experimental nuclear reaction data around the world. According to Table 1, the upstream spectrum with a relative difference of 13.07% in comparing the EXFOR data is the most appropriate spectrum to utilize, for which a cold neutron background should be removed. The result of employing the downstream region of the spectrum yielded 22.16%. Even though this error is higher than that of the upstream part, it is still preferable than employing the entire spectrum with an error of 26.43%. According to Figs. 5 and 6, the presence of a wide peak in the cold region of the spectrum, as well as a high neutron cross-section in this energy region can be a justification for the negative effect of the cold part of the spectrum on values.

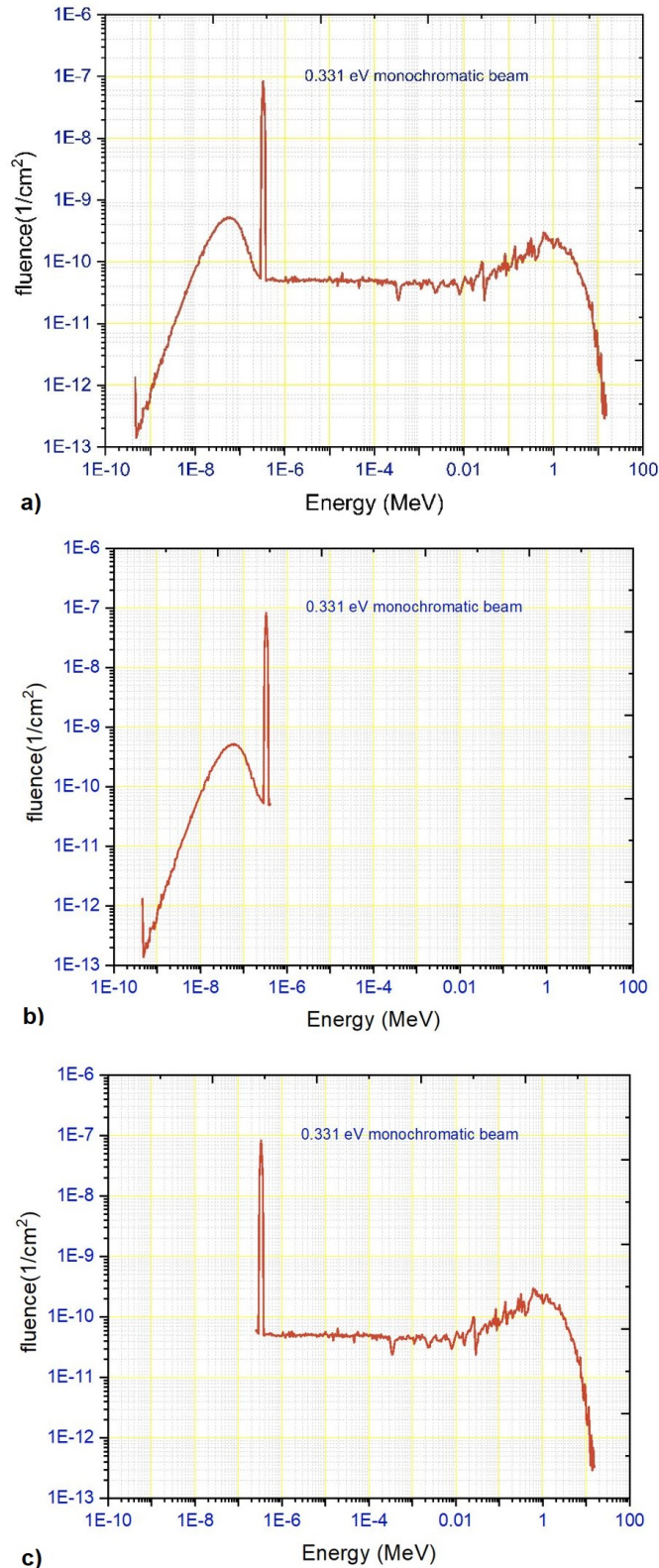


Figure 6: a) full neutron energy spectrum, b) downstream of mono-peak, c) upstream of mono-peak with the energy of 0.331 eV, at end of the D beam tube after the second collimator.

3 Results and Discussion

Figure 6 shows the neutron energy spectrum at the end of the D-beam tube after the second collimator which is ob-

tained from previous studies (Gholamzadeh et al., 2018). The orientation of the PG crystal has been chosen so that its mono-energetic peak is at 0.331 eV. Moreover, the spectra with upstream and downstream sections of mono-peak are depicted. There is a monochromatic peak with a substantially higher flux than the background spectrum at the energy chosen by the crystal. However, there may be disturbances in the monochromatic spectrum's performance due to the existence of the backgrounds in the different range of energies.

Table 2 also reports the removal of cold neutrons useful for measuring neutron cross-section at the energy of 0.083 eV with a relative discrepancy of 1.43%. However, unlike the energy of 0.331 eV, using the downstream section (8.40%) rather than the entire spectrum (6.34%) is not recommended in this energy. These findings suggest that filtering contaminants do not always assist in bringing results closer to libraries.

On the other hand, the results for neutron beams with a monochromatic peak at 0.036, 0.020, and 0.013 eV demonstrate the lowest relative difference in comparing the downstream spectrum and the EXFOR data, which are equal to 3.15%, 0.73%, and 1.37% respectively. However, the use of the full spectrum is more likely for the monochromatic peak at 0.036 which denotes the favorable impact of background presence on the cross section's values. Indeed, it behaves in such a way that the neutron spectrum section before and after the mono-energetic peak neutralizes each other in the reaction rate. Additionally, using the upstream spectrum is not recommended due to the greater relative difference than the full energy spectrum in the mentioned cases.

The calculated neutron radiative capture cross-sections for natural indium including two isotopes of In-115 and In-113 by several spectra with mono-peak at 0.331 eV are summarized in Table 6. Here, the upstream spectrum has the lowest relative difference of 5.69% in comparing the EXFOR data. Therefore, removing of cold neutron background is suggested for this purpose which is the same as the gold sample at the monochromatic peak of 0.331 eV.

Investigation of the appropriate spectrum for calculating the microscopic neutron radiative capture cross-section of rhodium (Rh-103) shows the different results which are given in Table 7. According to the results, the upstream spectrum has a lower relative difference in comparing the EXFOR data which means cold filters are beneficial. also, the full spectrum itself seems to be better than the downstream section.

The calculated cross-sections for $^{197}\text{Au}(n, \gamma)^{198}\text{Au}$ in this study are compared to other experimental data from around the world in Fig. 7. According to this graph, in the case of utilizing the full output neutron spectrum of channel D of the TRR to measure the cross-section, the data will have a significant relative discrepancy in some energies compared to other values throughout the world. Self-absorption, scattering, characteristics of neutron spectrum and its flux, and other factors can account for the differences in this comparison. At energies of 0.013, 0.020, and 0.331 eV the discrepancy in results is more obvious than at

Table 1: The calculation of microscopic cross-section for Au-197 sample by monochromatic neutron beam with the peak at 0.331 eV.

Neutron beam	Fluence at sample (cm^{-2})	(n, γ) reaction density (atoms.cm^{-3})	Microscopic cross-section (b)	EXFOR library (b)	Relative difference with EXFOR (%)
Mono-energetic	8.62×10^{-2}	2.82	32.8		6.74
Full spectrum	8.66×10^{-2}	3.36	38.8		26.43
Upstream of mono-peak	8.65×10^{-2}	3.00	34.7	30.7	13.07
Downstream of mono-peak	8.62×10^{-2}	3.23	37.5		22.16

Table 2: The calculation of microscopic cross-section for Au-197 sample by monochromatic neutron beam with the peak at 0.083 eV.

Neutron beam	Fluence at sample (cm^{-2})	(n, γ) reaction density (atoms.cm^{-3})	Microscopic cross-section (b)	EXFOR library (b)	Relative difference with EXFOR (%)
Mono-energetic	8.66×10^{-2}	4.96	57.26		2.99
Full spectrum	8.69×10^{-2}	5.14	59.13		6.34
Upstream of mono-peak	8.69×10^{-2}	4.90	56.39	55.6	1.43
Downstream of mono-peak	8.66×10^{-2}	5.22	60.27		8.40

Table 3: The calculation of microscopic cross-section for Au-197 sample by monochromatic neutron beam with the peak at 0.036 eV.

Neutron beam	Fluence at sample (cm^{-2})	(n, γ) reaction density (atoms.cm^{-3})	Microscopic cross-section (b)	EXFOR library (b)	Relative difference with EXFOR (%)
Mono-energetic	8.72×10^{-2}	7.27	83.39		0.72
Full spectrum	8.74×10^{-2}	7.04	80.57		2.69
Upstream of mono-peak	8.74×10^{-2}	6.94	79.44	82.8	4.06
Downstream of mono-peak	8.72×10^{-2}	7.45	85.41		3.15

Table 4: The calculation of microscopic cross-section for Au-197 sample by monochromatic neutron beam with the peak at 0.020 eV.

Neutron beam	Fluence at sample (cm^{-2})	(n, γ) reaction density (atoms.cm^{-3})	Microscopic cross-section (b)	EXFOR library (b)	Relative difference with EXFOR (%)
Mono-energetic	8.78×10^{-2}	9.65	109.94		0.86
Full spectrum	8.80×10^{-2}	9.01	102.43		7.64
Upstream of mono-peak	8.80×10^{-2}	8.96	101.82	110.9	8.19
Downstream of mono-peak	8.78×10^{-2}	9.81	111.71		0.73

Table 5: The calculation of microscopic cross-section for Au-197 sample by monochromatic neutron beam with the peak at 0.013 eV.

Neutron beam	Fluence at sample (cm^{-2})	(n, γ) reaction density (atoms.cm^{-3})	Microscopic cross-section (b)	EXFOR library (b)	Relative difference with EXFOR (%)
Mono-energetic	8.82×10^{-2}	11.78	133.45		2.66
Full spectrum	8.84×10^{-2}	10.74	121.57		11.33
Upstream of mono-peak	8.83×10^{-2}	10.72	121.30	137.1	11.53
Downstream of mono-peak	8.83×10^{-2}	11.94	135.22		1.37

Table 6: The calculation of microscopic cross-section for natural In by monochromatic neutron beam with the peak at 0.331 eV.

Neutron beam	Fluence at sample (cm^{-2})	(n, γ) reaction density (atoms.cm^{-3})	Microscopic cross-section (b)	EXFOR library (b)	Relative difference with EXFOR (%)
Mono-energetic	8.61×10^{-2}	7.67	89.19		3.36
Full spectrum	8.64×10^{-2}	8.34	96.51		11.85
Upstream of mono-peak	8.64×10^{-2}	7.88	91.20	86.29	5.69
Downstream of mono-peak	8.61×10^{-2}	8.27	96.02		11.28

Table 7: The calculation of microscopic cross-section for Rh-103 sample by monochromatic neutron beam with the peak at 0.331 eV.

Neutron beam	Fluence at sample (cm^{-2})	(n, γ) reaction density (atoms.cm^{-3})	Microscopic cross-section (b)	EXFOR library (b)	Relative difference with EXFOR (%)
Mono-energetic	8.60×10^{-2}	6.20	72.12		6.30
Full spectrum	8.64×10^{-2}	6.29	72.81		7.31
Upstream of mono-peak	8.63×10^{-2}	5.91	68.50	67.85	0.96
Downstream of mono-peak	8.60×10^{-2}	6.59	76.63		12.95

other energies, and there is a significant gap between data from this work and the experimental library. Therefore, different parts of the full neutron spectrum were used as sources so that it may be possible to measure more accurate cross-section values by determining neutron filtration in the NPD facility.

The cross-sections derived using the downstream spectrum (removing fast neutron background) are given in Fig. 8 compared to EXFOR data. We can notice the good influence of removing fast neutron background on the data findings by comparing this graph to Fig. 7. However, the data will still be far from the desired outcomes at higher energies, which removing cold background in this region is recommended.

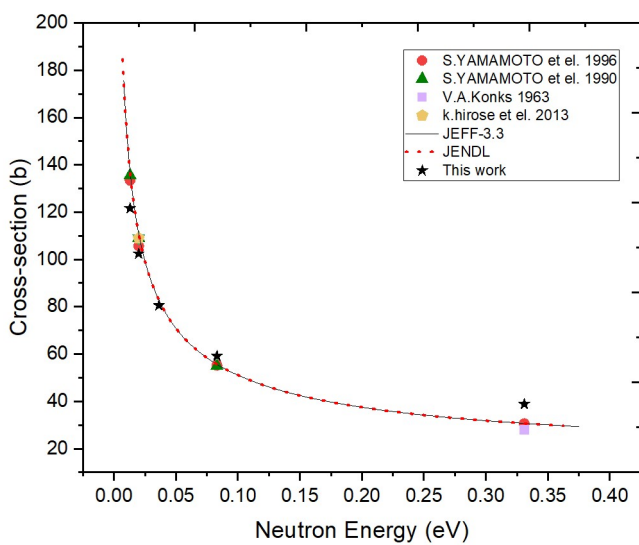


Figure 7: The comparison of $^{197}\text{Au}(n,\gamma)^{198}\text{Au}$ cross-section calculated by full neutron spectrum of channel D of the TRR with other experimental data in the world.

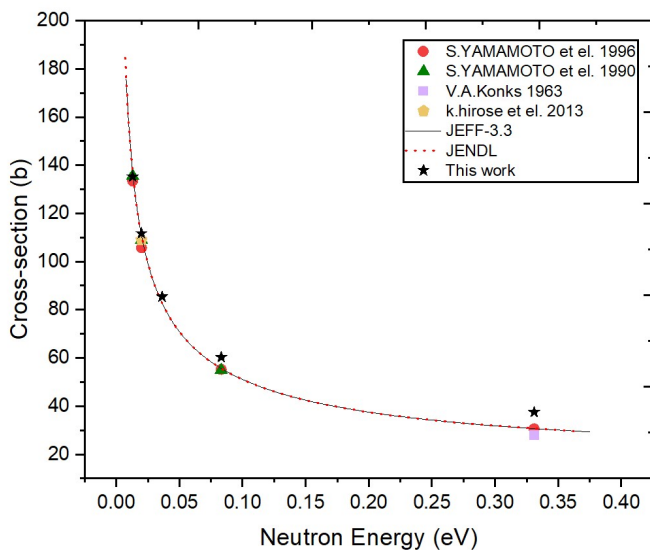


Figure 8: The comparison of $^{197}\text{Au}(n,\gamma)^{198}\text{Au}$ cross-section calculated downstream of mono-energetic neutron beam from channel D of the TRR with other experimental data in the world.

4 Conclusions

The neutron cross-section has been constantly studied to advance neutron research and applications. The development of radiation centers is significantly influenced by the precision of a material's neutron cross-section. In addition, the computational procedures provide us to evaluate a nuclear facility as completely safe without high-cost expenses on such systems' manufacturing before their optimization. NPD facility of the TRR is equipped with PG monochromator, suitable for measuring neutron cross-section. The output neutron spectrum of this beam has a variety of neutron backgrounds in addition to the monochromatic peak. In this work, the impact of different region of the neutron background being either present or absent on the (n,γ) cross sections of materials has been examined and also the weight of such backgrounds in the measurement precision has been evaluated. MCNPX, a Monte Carlo-based code has been used to simulate the TRR cross-section measurement system and to calculate the (n,γ) reaction rates of Au, In, and Rh sample materials. This code provides reaction rates using the stored cross-sections of the code libraries and it cannot determine the cross-section on its own. These reaction rates could differ proportionally to the system's circumstances and characteristics, including geometry, neutron flux, etc. According to the results, the impact of neutron background for determining the (n,γ) cross-section of different isotopes might vary. However, removing fast neutron background is often recommended which results in a mean relative difference of 7.16% in comparing EXFOR data for Au sample only. Removing the cold neutron background from the spectrum is also useful in providing differences of less than 15% and is preferable in some cases, while the average difference for Au samples in all energies is 7.65%.

For this reason, it can be examined in the upcoming works using simulation codes to design and provide an appropriate neutron filter more accurately for the NPD facility to measure the thermal neutron cross-section. Sapphire fast neutron filter due to the references has lots of the desired characters to be taken under consideration for NPD facility.

Consequently, it is recommended that the neutron cross-section be simulated and compared to single-energy before any measurement for each material. It causes to guide the system operator to determine which neutron filter may be required to enhance the measurement accuracy in the presence of the neutron backgrounds. The results of this study will be employed in the future for both benchmarking experimental data and designing a crystal filter to optimize the neutron spectrum of the TRR NPD facility for the cross-section measurement.

Conflict of Interest

The authors declare no potential conflict of interest regarding the publication of this work.

References

- Adib, M. (2005). Cross-section of single-crystal materials used as thermal neutron filters.
- Adib, M., Habib, N., Bashter, I., et al. (2011). Mgo single-crystal as an efficient thermal neutron filter. *Annals of Nuclear Energy*, 38(12):2673–2679.
- Adib, M., Habib, N., Kilany, M., et al. (2004). Neutron transmission through crystalline Fe.
- Adib, M. and Kilany, M. (2003). On the use of bismuth as a neutron filter. *Radiation Physics and Chemistry*, 66(2):81–88.
- Adib, M., Naguib, K., Ashry, A., et al. (2002). On the use of lead as a neutron filter. *Annals of Nuclear Energy*, 29(9):1119–1130.
- Brugger, R. M. (1976). A single crystal silicon thermal neutron filter. *Nuclear Instruments and Methods*, 135(2):289–291.
- Celenk, I., Demirel, H., and Özmen, A. (1991). Measurement of macroscopic and microscopic thermal neutron cross sections of V, Co, Cu, In, Dy and Au using neutron self-absorption properties. *Journal of Radioanalytical and Nuclear Chemistry*, 148(2):393–401.
- Cierjacks, S., Shibata, K., and Issy-les Moulineaux, F. (1994). *Blind Intercomparison of Nuclear Models for Predicting Charged Particle Emission, NEA/NSC-DOC93-4*. Nuclear Energy Agency, OECD.
- Dastjerdi, M. C., Khalafi, H., Kasesaz, Y., et al. (2016). Design, construction and characterization of a new neutron beam for neutron radiography at the Tehran Research Reactor. *Nuclear Instruments and Methods in Physics Research Section A: Accelerators, Spectrometers, Detectors and Associated Equipment*, 818:1–8.
- Drozdowicz, K. (1989). Energy-dependent scattering cross section of plexiglass for thermal neutrons. Technical report, Chalmers Univ. of Tech.
- El Abd, A., Taha, G., and Ellithi, A. (2017). A method for measuring macroscopic cross-sections for thermal neutrons. *Applied Radiation and Isotopes*, 128:318–327.
- ENDF (2021). ENDF: Evaluated Nuclear Data File, <https://www-nds.iaea.org/exfor/endl.htm#1>. Technical report.
- Gholamzadeh, Z., Bavarnegin, E., Racht, M. L., et al. (2018). Modeling of neutron diffractometry facility of Tehran Research Reactor using Vitess 3.3 a and MCNPX codes. *Nuclear Engineering and Technology*, 50(1):151–158.
- Hançerlioğullari, A., KORKUT, T., and MADEE, Y. G. A. (2017). The Neutron Macroscopic Cross Sections Calculation of Some Minerals by Using FLUKA Monte Carlo Method. *The Online Journal of Science and Technology-July*, 7(3).
- Harvey, J., MOOK, H., HILL, N., et al. (1988). Nuclear data for science and technology.
- Huang, X., Lu, H., Zhao, W., et al. (1998). Neutron activation cross section measurements and evaluations in CIAE. Technical report, International Atomic Energy Agency.
- Jacobson, L. A. (1988). Macroscopic thermal neutron capture cross section measurements. *IEEE Transactions on Nuclear Science*, 35(1):817–821.
- Kobayashi, H., Wakao, H., Ikeda, Y., et al. (1992). Macroscopic cross section measurements and defect detection in materials using neutron radiography technique. *Journal of Nuclear Science and Technology*, 29(11):1045–1053.
- Lamarsh, J. R., Baratta, A. J., et al. (2001). *Introduction to nuclear engineering*, volume 3. Prentice hall Upper Saddle River, NJ.
- Pelowitz, D. B. et al. (2005). MCNPXTM user's manual. *Los Alamos National Laboratory, Los Alamos*, 5:369.
- Pelowitz, D. B. et al. (2011). MCNPXTM user's manual. *Los Alamos National Laboratory, Los Alamos*, 5:369.
- Rubbia, C., Roche, C., Rubio, J. A., et al. (1995). Conceptual design of a fast neutron operated high power energy amplifier. Technical report.
- Steele, E. L. and Meinke, W. W. (1962). Determination of rhodium by thermal neutron activation analysis using g-ray spectrometry. *Analytica Chimica Acta*, 26:269–274.

©2023 by the journal.

RPE is licensed under a [Creative Commons Attribution-NonCommercial 4.0 International License](https://creativecommons.org/licenses/by-nc/4.0/) (CC BY-NC 4.0).



To cite this article:

Pazoki, M., Jafari, H., Gholamzadeh, Z. (2023). Studying the effect of backgrounds on the determination of radiative thermal neutron capture cross-section in the Neutron Powder Diffraction facility of the Tehran Research Reactor. *Radiation Physics and Engineering*, 4(2), 9-17.

DOI: [10.22034/rpe.2022.349750.1094](https://doi.org/10.22034/rpe.2022.349750.1094)

To link to this article: <https://doi.org/10.22034/rpe.2022.349750.1094>